0.997; **2** $\sigma^{\alpha C^+}$, 4.71, 0.25, 12.56, 0.19, 0.994; **3**, σ^+, 6.14, 0.25, 9.81, 0.15, 0.997; **3**, $\sigma^{\alpha C^+}$, 4.71, 0.25, 10.56, 0.19, 0.994. For the combined series of ions: **1–3**, σ^+, 6.17, 0.41, 10.48, 0.25, 0.966; **1–3**, $\sigma^{\alpha C^+}$, 4.73, 0.33, 11.22, 0.26, 0.962; **2, 4** (45°), σ^+, 0.78, 0.20, 4.17, 0.12, 0.777; **2, 4**, $\sigma^{\alpha C^+}$, 0.58, 0.16, 4.27, 0.12, 0.752; **3, 5** (30°), σ^+, 0.19, 0.24, –0.36, 0.15, 0.244; **3, 5**, $\sigma^{\alpha C^+}$, 0.15, 0.19, –0.33, 0.14, 0.252.

Ion Precursors. The tertiary alcohol precursors for **1–3** and **5** were all prepared by standard Grignard procedures from the corresponding alkanones or were available from a previous study.[7] Physical constants of these materials are available in the literature (H. C. Brown et al.[3]) and we have measured their ^{13}C spectra.

Preparation of Ions. The ions were prepared in known concentration from the tertiary alcohols either by direct addition to the precooled (–78 °C) acid solution or by addition of a solution (–10 to –70 °C) of the alcohol to the precooled acid solution. Ion, concentration, superacid, temperature of ^{13}C measurement: **1** (R = *p*-OCH_3) 0.46 M, HSO_3F, –25 °C, (R = *p*-CH_3) 0.78, HSO_3F, –70 °C, (R = *p*-H) 0.34, HSO_3F/SbF_5, –65 °C, (R = *p*-F) 0.35, HSO_3F/SbF_5, –65 °C, (R = *p*-CF_3) 0.60, HSO_3F/SbF_5, –40 °C, (R = 3,5-$(CF_3)_2$) 0.33, HSO_3F/SbF_5, –65 °C; **2** (R = *p*-OCH_3) 0.77, HSO_3F, –60 °C, (R = *p*-CH_3) 0.89, HSO_3F, –60 °C, (R = *p*-H) 0.85, HSO_3F, –60 °C, (R = *p*-Cl) 0.75, HSO_3F, –60 °C, (R : *p*-CF_3) 0.54, HSO_3F/SbF_5, –70 °C, (R = 3,5-$(CF_3)_2$) 0.45, HSO_3F/SbF_5, –70 °C; **3** (R = *p*-OCH_3) 0.46, HSO_3F, –25 °C, (R = *p*-CH_3) 0.56, HSO_3F, –25 °C, (R = *p*-H) 0.64, HSO_3F, –25 °C, (R = *p*-Cl) 0.54, HSO_3F, –25 °C, (R = *p*-CF_3) 0.47, HSO_3F, –30 °C, (R = 3,5-$(CF_3)_2$) 0.38, HSO_3F, –30 °C; **4** (all HSO_3F/SbF_5, –40 °C)[7] (R = *p*-OCH_3) 0.44, (R = *p*-CH_3) 0.48, (R = *p*-H) 0.51, (R = *p*-F) 0.51, (R = *p*-CF_3) 0.38, (R = 3,5-$(CF_3)_2$ 0.33; **5** (R = *p*-OCH_3) 0.77, HSO_3F, –60 °C, (R = *p*-CH_3) 0.84, HSO_3F, –60 °C, (R = *p*-H) 0.91, HSO_3F, –60 °C, (R = *p*-Cl) 0.75, HSO_3F, –60 °C, (R = *p*-CF_3) 0.53, HSO_3F/SbF_5, –60 °C, (R = 3,5-$(CF_3)_2$) 0.35, HSO_3F/SbF_5, –60 °C.

Acknowledgment. This work was supported by the Australian Research Grants Committee.

Transport of Photoproduced Ions in Water in Oil Microemulsions: Movement of Ions from One Water Pool to Another[1]

S. S. Atik and J. K. Thomas*

Contribution from the Department of Chemistry, University of Notre Dame, Notre Dame, Indiana 46556. *Received December 1, 1980*

Abstract: Pulsed laser photolysis techniques were used to study the following reactions in reversed micelles of AOT/alkane/water:

$$Ru^{II}(bpy)_3^* + Fe(CN)_6^{3-} \rightarrow Ru^{III}(bpy)_3 + Fe(CN)_6^{4-}$$

$$Ru^{II}(bpy)_3^* + MV^{2+} \rightarrow Ru^{III}(bpy)_3 + MV^{+}$$

$$PTS^T + FS \rightarrow PTS$$

$$PTS^T + Cu^{2+} \rightarrow PTS$$

where $Ru^{II}(bpy)_3$ and MV^{2+} represent ruthenium tris(bipyridyl) and methyl viologen, respectively, while PTS^T and FS represent the triplet excited state of pyrenetetrasulfonic acid and Fremy's salt, respectively. These ionic reactants are associated only with the water pools of the reversed micelle systems, a situation which introduces unusual features into the kinetics. Analysis of the kinetics shows that the reactants distribute themselves among the micelles according to a Poisson rather than a geometric distribution. Analysis of the decay kinetics under various conditions enables the measurement of the exchange rate of ions among micelles to be measured. This ion exchange occurs only on collision of water pools, and the effectiveness of exchange is 1% or less in a simple AOT system for both Cu^{2+} and the anionic Fremy's salt. Various additives such as benzyl alcohol markedly increase the efficiency of ion exchange, while solutes such as benzene decrease it. These data are discussed in terms of the interactions of the additives with the micellar head groups.

The last few years have seen considerable activity in the area of micellar catalysis. In particular, catalysis in reversed micelles or microemulsions has received detailed attention[2,3] as these systems strongly catalyze many reactions. Much is known about the structure of specific systems,[4–6] and a reasonable description of reaction sites can be put forward with some confidence. Basically, these systems consist of pools of water (radii 15–150 Å) stabilized in a bulk hydrocarbon by a suitable surfactant, e.g., disodium diisooctylsulfosuccinate (AOT), or a surfactant–co-surfactant pair, e.g., potassium oleate/hexanol or cetyltrimethylammonium bromide (CTAB)/hexanol. The surfactants are located at the water–hydrocarbon boundary. The nature of the water has received some attention,[7] and it is found that many physical measurements indicate that the properties reminiscent of bulk water are only approached in larger water bubbles.

Micellar systems are of general interest as suitable vehicles for promotion of photochemical studies.[8] The correct selection of a system can lead to large yields of photoproduced ions which are stabilized by the micelle system.[9,10] Some work in reversed micelles or microemulsions[11–13] suggests that these systems may

(1) We thank the NSF for support of this research via Grant CHE-78-24867.

(2) Fendler, J. H. *Acc. Chem. Res.* **1976**, *9*, 1953.
(3) Menger, F. *Acc. Chem. Res.* **1979**, *12*, 111.
(4) Zulauf, M.; Eicke, H. F. *J. Phys. Chem.* **1979**, *83*, 450.
(5) Shinoda, K.; Friberg, S. *Adv. Colloid Interface Sci.* **1975**, *4*, 281.
(6) Bansal, V. K.; Chinnaswamy, K.; Ramachandran, C.; Shah, D. O. *J. Colloid Interface Sci.* **1979**, *72*, 524.
(7) Wong, M.; Thomas, J. K.; Grätzel, M. *J. Am. Chem. Soc.* **1976**, *98*, 2391.
(8) Thomas, J. K.; Almgren, M. In "Solution Chemistry of Surfactants"; Mittal, K. L., Ed.; Plenum Press: New York, 1979; p 559.
(9) Räzem, B.; Wong, M.; Thomas, J. K. *J. Am. Chem. Soc.* **1978**, *100*, 1679.
(10) Kiwi, J.; Grätzel, M. *J. Am. Chem. Soc.* **1978**, *100*, 6314.
(11) Matsuo, T.; Nagamura, T.; Itoh, K.; Nishijima, T. *Mem. Fac. Eng., Kyushu Univ.* **1980**, *40*, 25.
(12) Ford, W. E.; Otvos, J. W.; Calvin, M. *Nature (London)* **1978**, *274*, 507.

0002-7863/81/1503-3543$01.25/0

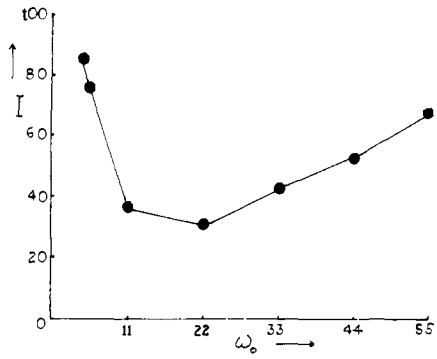

Figure 1. Effect of water content W_0, where $W_0 = [H_2O]/[AOT]$ on the $Ru^{II}(bpy)_3$ in the system: $Ru^{II}(bpy)_3$, 5.0×10^{-5} M; $K_3Fe(CN)_6$, 1.0×10^{-3} M; 0.2 M AOT in heptane. Solutions are dearated. $Ru^{II}(bpy)_3$ was excited at $\lambda = 4600$ Å and the luminescence measured at $\lambda = 6450$ Å.

play an important role as models for photostorage assemblies and photosynthesis.

An important feature of beneficial micellar effects is the rapid and efficient removal of the photoproducts, in particular ions from the original reaction site, i.e., micelle. In conventional Hartley micelles, i.e., where the bulk phase is water, the products are ejected into the aqueous phase where they may subsequently react with water soluble scavengers or reenter other micelles.[14] In microemulsions transport of an ionic reaction product from one micelle to another is not as easily achieved due to the low affinity of the ionic species for the bulk hydrocarbon. A recent estimate[15] indicates that the transport of ions between water droplets in a reversed micelle system takes many microseconds. The purpose of this work is to investigate reactions of several photoinduced ionic systems, leading to data which give direct measurements of ion transport in these systems and suggest a mechanism for the process.

Experimental Section

Fluorescence spectra were measured on a Perkin–Elmer MPF44 spectrophotometer. Life times of excited states and spectra of short-lived intermediates were measured on a laser flash photolysis apparatus. The laser source was a Korad K1Q, Q-switched, frequency doubled ruby laser giving 20-ns, 0.1-J pulses of light, $\lambda = 3471$ Å. Signals from the irradiated sample, either in the emissive or in absorptive mode, were monitored by a Tektronix 7912AD transient capture device and subsequently transported to a Tektronix 4051 computer for processing and display.

The chemicals were obtained from the following sources and purified as in previous papers: cetyltrimethylammonium bromide (CTAB) and oleic acid from Sigma Chemicals, disodium diisooctylsulfosuccinate (AOT) from Fluka Chemicals, Fremy's salt, $(KSO_3)_2NO(FS)$, from Alfa Products, tetrasodium 1,3,6,8-pyrenetetrasulfonate (PTS) and pyrene from Eastman Chemicals. Other chemicals were reagent or analytical grade.

Reversed micelles of 0.2 M AOT in heptane, having different values of W_0 ([water]/[surfactant]) and containing the appropriate concentration of the reactants, were prepared as follows: To 4 mL of 0.5 M AOT in heptane, 50 μL of 0.1 M PTS or ruthenium tris(bipyridyl) $Ru^{II}(bpy)_3$ in water is added by using a microsyringe. The solution is then mixed with a vortex mixer until clarity is effected. To this solution a predetermined aqueous volume of 0.1 M $K_3Fe(nCN)_6$ (or 0.1 M Fremy's salt in 0.1 M NaOH) is added, followed by addition of a calculated volume of water to give a solution with the exact value of W_0. The mixture is thoroughly vortex mixed again (for samples having $W_0 \geq 33$, warming is sometimes necessary) to ensure complete solubilization and achieve perfect visual clarity. Finally, the solution is diluted to a final volume of 10 mL with heptane.

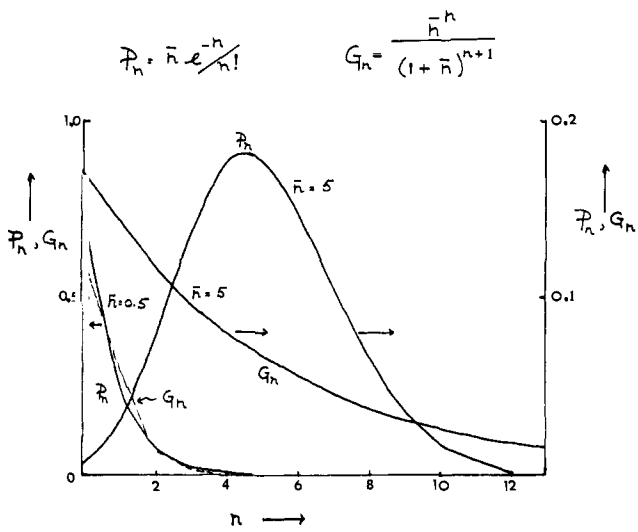

Figure 2. Poisson and geometric statistical probability distributions for different values of $\bar{n}$.

Before every spectroscopic measurement, samples were carefully and repeatedly outgassed by bubbling high quality oxygen-free N_2.

Results and Discussion

Steady-State Measurements. Figure 1 shows the effect of water content, given as $W_0 = [H_2O]/[AOT]$, on the fluorescence yield of $Ru^{II}(bpy)_3$, in the presence of 10^{-3} M potassium ferricyanide, in the system AOT–heptane–water. Increasing the water content, with $W_0 = 5.5$, leads to an initial decrease in the $Ru^{II}(bpy)_3$ fluorescence yield, followed by an increase at high W_0. It is noted that dilution of the AOT–$Ru^{II}(bpy)_3$–$Fe(CN)_6^{3-}$ system with heptane does not change the decay kinetics of excited $Ru^{II}(bpy)_3$. This suggests that the reacting species are associated only with the water pools in keeping with their strongly ionic character. The data are interpreted as a variation in the quenching efficiency of $Fe(CN)_6^{3-}$ ions with the excited $Ru^{II}(bpy)_3$. At low water content, small W_0, the nature of the water pools deviates quite markedly from that of bulk water, and the aqueous environment is quite rigid,[7] i.e., low quenching efficiency. Increasing the water content leads to a decrease in the rigidity of the water region which, in turn, leads to a more rapid quenching of excited $Ru^{II}(bpy)_3$ by $Fe(CN)_6^{3-}$. Continued increase of the water content leads to larger water pools with a corresponding decrease in the local concentrations of excited $Ru^{II}(bpy)_3$ and $Fe(CN)_6^{3-}$, which now leads to a slower reaction and a decrease in the quenching of excited $Ru^{II}(bpy)_3$.

Distribution of Reactants among Water Pools. One could envisage two possible statistical laws (Poisson and geometric) that govern the distribution of reactants amongst water pools or micelles. In aqueous solution it has been suggested that a geometric distribution is most appropriate in describing the arrangement of water insoluble solutes amongst micelles.[18] This is in direct contrast to many experimental observations that favor a Poisson distribution in these systems. However, to our knowledge, there are no reports of similar investigations in reversed micelles or microemulsions, where the distribution of ionic solutes amongst water pools has been considered. The main feature of the two distribution laws is that they have similar probability distributions for values of $\bar{n} < 1$, where $\bar{n}$ is [solute]/[micelle]. However, a distinct difference between these probability distribution functions becomes pronounced for $\bar{n} > 1$ (Figure 2). For large values of $\bar{n}$, according to Poisson statistics, the most probable occurrence of a water pool is that containing $\bar{n}$ number of solubilizates. On the other hand, according to the geometric distribution function, the highest probability is always associated with empty micelles or water pools, a feature which makes this type of distribution

(13) Costa, S.; Thomas, J. K., unpublished work.
(14) Almgren, M.; Grieser, F.; Thomas, J. K. *J. Am. Chem. Soc.* **1979**, *101*, 279.
(15) Robinson, B. H. *J. Chem. Soc., Faraday Trans. 1* **1979**, *75*, 481. Day, R. A.; Robinson, B.-H.; Clarke, J. H. R.; Doherty, J. V. *J. Chem. Soc., Faraday Trans. 1* **1979**, *75*, 132.
(16) Kalyanasundaram, K.; Grätzel, M.; Thomas, J. K. *J. Am. Chem. Soc.* **1975**, *97*, 3915.
(17) Atik, S. S.; Kwan, C. L.; Singer, L. *J. Am. Chem. Soc.* **1979**, *101*, 5696.
(18) Dorrance, R. C.; Hunter, T. F. *J. Chem. Soc., Faraday Trans. 1* **1977**, *73*, 1891.
(19) Atik, S. S.; Nam, N.; Singer, L. A. *Chem. Phys. Lett.* **1979**, *67*, 75.

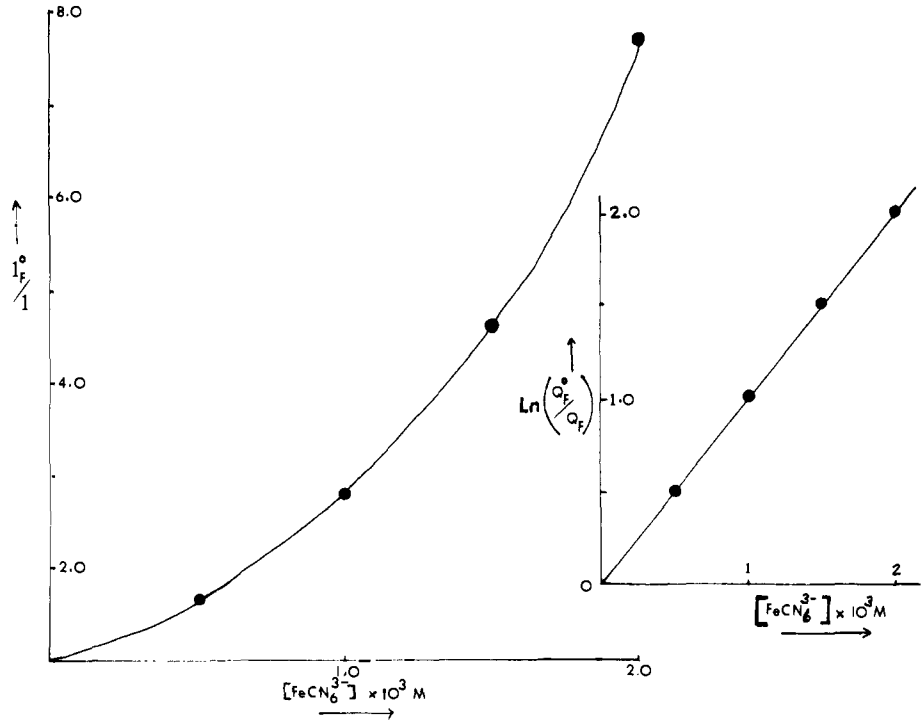

Figure 3. Stern–Volmer-type plot for quenching of $Ru^{II}(bpy)_3$ fluorescence by $K_3Fe(CN)_6$ at a constant $W_0 = 11$. Solution 5.0×10^{-5} M $Ru^{II}(bpy)_3$–0.2 M AOT–heptane deoxygenated. $Ru^{III}(bpy)_3$ excited at $\lambda = 4600$ Å and luminescence observed at $\lambda = 6450$ Å. Insert: Plot of ln (ϕ_F^0/ϕ_F) vs. $[Fe(CN)_6^{3-}]$.

awkward and unrealistic. Here, and in the following section, the predictions of a kinetic model based on the two different statistical functions are tested against the experimental data.

Figure 3 shows a Stern–Volmer plot for the quenching of $Ru^{II}(bpy)_3$ with $Fe(CN)_6^{3-}$ at constant W_0 ($W_0 = 11$). The severe upward curvature of this plot clearly reflects the inhomogeneous distribution of the quencher molecules among the water pools where the fluorescence quenching reaction is expected to occur.

A steady-state expression which uses Poisson statistics to describe the distribution of quenchers among discrete particles has been derived and is given by[20]

$$\frac{\phi_F}{\phi_F^0} = \sum_{n=0}^{\infty} \frac{\alpha_n}{1 + nA} \tag{1}$$

where α_n is the statistical probability weighting factor for a water pool containing n quenchers, A is k_q/k_1, where k_q is a specific quenching rate constant for a water pool containing only one quencher and k_1 is the sum of all first-order rate processes leading to the deactivation of the excited state in the absence of quencher.

For a distribution of quenchers that follow Poisson statistics, the corresponding expression is

$$\frac{\phi_F}{\phi_F^0} = \sum_{n=0}^{\infty} \frac{n^{-n}e^{-\bar{n}}/n!}{1 + nA} \tag{2}$$

where $\bar{n}$ is the average number of quenchers associated with a water pool ($\bar{n} = [Q]_T/[WP]_T$).

On the other hand, a geometric distribution gives

$$\frac{\phi_F}{\phi_F^0} = \sum_{n=0}^{\infty} \frac{n^{-n}/(1 + \bar{n})^{n+1}}{1 + nA} \tag{3}$$

Both theoretical expressions 2 and 3 would predict a positive deivation from linearity for a S-V plot of ϕ_F^0/ϕ_F vs. $[Q]_T$. However, a marked difference between (2) and (3) is predicted in the limiting case where $A \gg 1$ (i.e., $k_q \gg k_1$) when one quencher in a water pool is sufficient to quench an excited probe in a very short time (static) compared to its normal fluorescence lifetime. Under this condition, when ≥95% of the fluorescence is emitted from water pools that contain only an excited probe, a Poisson distribution predicts from eq 2

$$\phi_F/\phi_F^0 = e^{-\bar{n}} \tag{4}$$

while from eq 3 a geometric distribution gives

$$\phi_F/\phi_F^0 = 1/(1 + \bar{n}) \tag{5}$$

The linearity of the plot shown in Figure 3 (inset) strongly supports a Poisson distribution and argues against a geometric one which predicts a linear relationship between ϕ_F^0/ϕ_F and $\bar{n}$ or $[Q]_T$.

Applicability of eq 4 in describing the quenching of $Ru^{II}(bpy)_3$ luminescence by $Fe(CN)_6^{3-}$ in the AOT reversed micelle ($W_0 = 11$) system implies that $k_q \gg 1.54 \times 10^6$, i.e., $1/\tau$. An exact value for k_q can, however, be obtained from the analysis of the time-correlated luminescence as described in the next section. Furthermore, eq 4 also predicts that ln (ϕ_F^0/ϕ_F) is linearly related to the reciprocal of the [water pool] or $[WP]_T$ at constant $[Q]_T$. Figure 4 shows fluorescence quenching of 5.0×10^{-5} M $Ru^{II}(bpy)_3$ at constant $[Fe(CN)_6^{3-}] = 1.0 \times 10^{-3}$ M and $[H_2O]/[AOT] = 11$, while varying *both* $[H_2O]$ and [AOT]. A decrease in the efficiency of luminescence quenching is observed as the mean $Fe(CN)_6^{3-}$ occupancy level decreases as a result of increasing $[WP]_T$. Assuming spherical water pools, $[WP]_T$ can be expressed as

$$[WP]_T = 30(\%\ H_2O)/(4\pi R_w^3 N_0) \tag{6}$$

where R_w is the water pool radius.

Substitution in eq 4 gives

$$\ln (\phi_F^0/\phi_F) = (4/30)\pi R_w^3 N_0 [Q]_T (1/\%\ H_2O) \tag{7}$$

At fixed $[Q]_T$ and W_0 and varying [AOT], a plot of ln (ϕ_F^0/ϕ_F) vs. $(\%\ H_2O)^{-1}$ should be linear with a slope given by $(4/30)\pi R_w^3 N_0 [Q]_T$. Such a prediction would be observed if the radius of the water pools does not change under these conditions.

The insert in Figure 4 shows such a plot, but contrary to expectation two discernable linear regions are observed. However, the two regions are in accordance with eq 7 as they both pass

(20) Atik, S. S.; Singer, L. A. *Chem. Phys. Lett.* **1979**, *66*, 234.

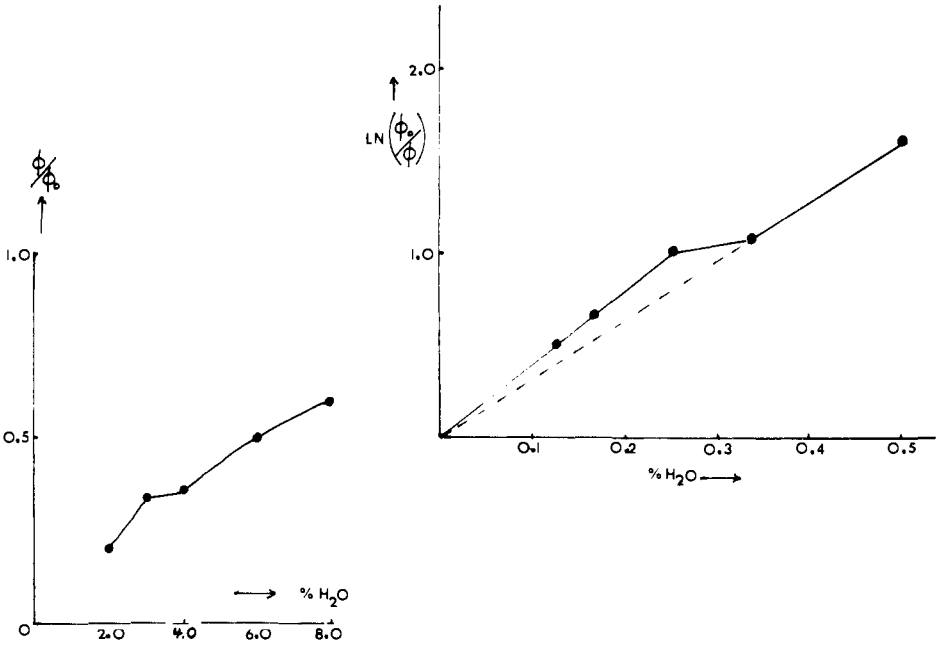

Figure 4. Variation in the efficiency of luminescence ϕ_F^0/ϕ_F in the system 5.0×10^{-5} M $Ru^{II}(bpy)_3$–1.0×10^{-3} M $K_3Fe(CN)_6$–0.2 M AOT in heptane under deoxygenated conditions, W_0 constant at 11 while varying both $[H_2O]$ and [AOT], vs. (% H_2O). Insert: logarithmic plot of luminescence efficiency vs. inverse of (% H_2O).

through the origin. According to eq 7 the observation of two linear regions implies a change in the radius of the spherical water pool as [AOT] is increased from 0.1 to 0.4 M, W_0 being maintained constant at $W_0 = 11$.

Analysis of the first region (0.2–0.4 M AOT) according to eq 7 yields R_w of 25 Å, while the second region, 0.1–0.15 M AOT, gives $R_w = 17$ Å.

Time Dependence of $Ru^{II}(bpy)_3$ Luminescence. In the preceding section steady-state data were found to be in good agreement with the predictions of a kinetic model based on Poisson statistics. The present time-correlated luminescence data were analyzed in an attempt to provide confirmatory evidence for the Poisson distribution. Figure 5 confirms these suggestions as it shows that the life time of excited $Ru^{II}(bpy)_3$, i.e., $Ru^{II}(bpy)_3$*, decreases in the presence of $Fe(CN)_6^{3-}$ (in water, the $k_q = 3.8 \times 10^{10}$ L M^{-1} s^{-1}). At low water content an initial rapid quenching of $Ru^{II}(bpy)_3$* is followed by subsequent slower decay which is not quenched. The rapid decay is due to a situation where $Ru^{II}(bpy)_3$* and $Fe(CN)_6^3$ occupy the same water pool, while the slower decay is due to isolated $Ru^{II}(bpy)_3$* in water pools which do not contain $Fe(CN)_6^{3-}$. A continued increase in water content up to $W_0 \sim 33$ leads at first to more rapid reaction. Beyond this point, the decay of $Ru^{II}(bpy)_3$* decreases and becomes a single exponential. This occurs in large water pools where the water pool concentration, [WP], is low so that all pools contain both $Ru^{II}(bpy)_3$* and $Fe(CN)_6^{3-}$, i.e., at high values of $\bar{n}$ and/or $k_q \leq k_1$.

Distribution of Reactants among the Water Pools. It has been suggested that the distribution of solutes amongst micelles follows a Poisson distribution[16,17] and also a geometric distribution.[18] The present data enable us to discuss this situation critically. Figure 5 shows the decay of $Ru^{II}(bpy)_3$* with time in the AOT–heptane–water system, in the presence of $Fe(CN)_6^{3-}$, at 5.0×10^{-4} and 1.5×10^{-3} M. The Appendix shows the forms of the distribution which lead to the following equations for the decay of $Ru^{II}(bpy)_3$* given by $I_F(t)$ in these systems. Poisson distribution:

$$I_F(t) = I_F(t = 0)e^{-[k_1 t + \bar{n}(1-e^{-k_q t})]} \qquad P_n = \bar{n}^n e^{-\bar{n}}/n! \qquad (8)$$

Geometric distribution:

$$I_F(t) = \frac{I_F(t = 0)e^{-k_1 t}}{1 + \bar{n}\,(1 - e^{-k_q t})} \qquad G_n = \frac{n^{-n}}{(1 + \bar{n})^{n+1}} \qquad (9)$$

The average [solute]/[micelle] or $\bar{n}$ is calculated by using Eicke's values for the concentration of water pools in these systems.[4] The solid curve shows the calculation for the Poisson distribution utilizing identical parameters at both $[Fe(CN)_6^{3-}]$. The parameters are $[Fe(CN)_6^{3-}] = 5 \times 10^{-4}$ M, $\bar{n} = 0.80$, $k_q = 6.0 \times 10^6$ s^{-1}, $k_1 = 1.54 \times 10^6$ s^{-1}, and $[Fe(CN)_6^{3-}] = 1.5 \times 10^{-3}$ M, $\bar{n} = 2.4$, $k_q = 6.0 \times 10^6$ s^{-1}, $k_1 = 1.54 \times 10^6$ s^{-1}.

The fit of the geometric distribution with the data cannot be made using identical parameters at both $[Fe(CN)_6^{3-}]$. The numbers giving best fits are $[Fe(CN)_6^{3-}] = 5 \times 10^{-4}$ M, $\bar{n} = 1.25$, $k_q = 4.5 \times 10^6$ s^{-1}, $k_1 = 1.54 \times 10^6$ s^{-1}, and $[Fe(CN)_6^{3-}] = 1.5 \times 10^{-3}$ M, $\bar{n} = 10.0$, $k_q = 2.0 \times 10^6$ s^{-1}, $k_1 = 1.54 \times 10^6$ s^{-1}.

We conclude that the Poisson distribution gives the best fit to our data, as in Figure 5B the solid lines of the Poisson distribution are a much better fit to the data than the dotted geometric distribution.

Table I. Parameters Obtained from the Luminescence Decay Analysis of 5.0×10^{-5} M $Ru^{II}(bpy)_3$–0.2 M AOT + Heptane–1.0×10^{-3} M $K_3Fe(CN)_6/N_2$[a]

W_0	$\bar{n}$	$k_1 \times 10^{-6}$, s^{-1}	$k_q \times 10^{-7}$, s^{-1}	R_w, Å (4)
11	0.90	1.54	1.7	24 (24)
22	1.65	1.54	0.65	38 (37)
33	7.00	1.54	0.075	51 (75)
44	(20)	1.54	0.0085	(108)
55	(28)	1.54	0.004	(133)

[a] $W_0 = [H_2O]/[AOT]$, $10(\%\ H_2O, v/v) = N_0[WP]_T(^4/_3 \pi R_W^3)$, $\bar{n} = [K_3Fe(CN)_6]/[WP]_T$, $R_W = [4.0\,(\%\ H_2O)/[WP]_T]^{1/3}$.

Table I shows the radii values calculated from our experiment at various W_0 along with those of Eicke which were determined by other techniques. Again the agreement is good and lends support to the kinetic processes used. Figure 6 shows the variation in R_w with W_0 for four microemulsions systems. The R_w are constant to within a factor 2 for all systems at a set W_0.

Exchange of Ions between Water Pools. The kinetics of exchange of ions between water pools was studied by utilizing the quenching of triplet excited states of pyrenetetrasulfonate (PTS) and PSA by Fremy's salt and cupric ions. All reactants are very polar, and reaction is confined to the water pools. Laser excitation of PTS gives rise to the singlet excited state which, within 10 ns, intersystem crosses to the triplet state PTS^T, which has a long lifetime, >1 ms. At low quencher concentration (in the AOT system) the kinetics follow a simple Stern–Volmer relationship as the quenching of excited PTS^T is via transport of quencher from one water pool to another. Typical data are shown in Figure 7

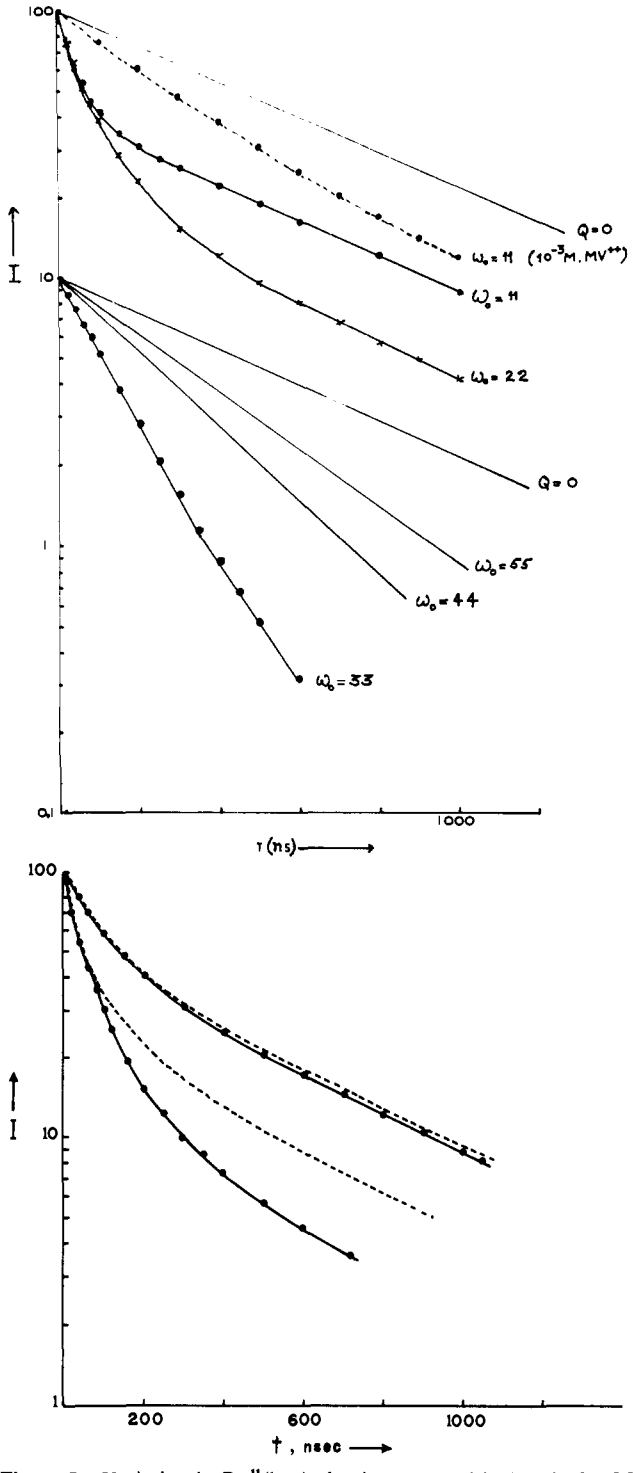

Figure 5. Variation in $Ru^{II}(bpy)_3$ luminescence with time in 0.2 M AOT/heptane–5.0×10^{-4} M $Ru^{II}(bpy)_3$, deoxygenated conditions, with varying W_0. (A) $K_3Fe(CN)_6$, 1.0×10^{-3} M; (B) fit of Poisson and geometric statistics with $W_0 = 22$; (1) 5.0×10^{-4} M $K_3Fe(CN)_6$, upper curves, (2) 1.5×10^{-3} M $K_3Fe(CN)_6$, lower curves. Solid line Poisson; dotted line geometric distribution. (1) Poisson distribution: $\bar{n} = 0.80$, $k_q = 6.0 \times 10^5$ s^{-1}, $k_1 = 1.54 \times 10^6$ s^{-1}. Geometric distribution: $\bar{n} = 1.25$, $k_q = 4.5 \times 10^6$ s^{-1}, $k_1 = 1.54 \times 10^6$ s^{-1}. (2) Poisson distribution: $\bar{n} = 2.2$, $k_q = 6.0 \times 10^6$ s^{-1}, $k_1 = 1.54 \times 10^6$ s^{-1}. Geometric distribution: $\bar{n} = 3.75$, $k_q = 4.5 \times 10^6$ s^{-1}, $k_1 = 1.54 \times 10^6$ s^{-1}. Solid decay curves are computed with the above parameters.

where k_q for Cu^{2+} is 2.0×10^7 L M^{-1} s^{-1}, and k_q for Fremy's salt is 1.2×10^7 L M^{-1} s^{-1}.

At higher quencher concentration the kinetics are not simple, and the state of occupancy of the pools must be considered. Typical data are shown in Figure 8 for several W_0 and Fremy's salt concentrations. The kinetics exhibit an initial rapid nonexponential decay followed by a slower exponential decay. A simple consideration of the distribution of PTS^T and quencher among the water pools explains the data. The [PTS] and hence [PTS^T] is much less than [water pools], while [Q] ≥ [water pools]. Hence Q will distribute among the water pools according to a Poisson distribution, leaving some pools void of Q and some pools occupied by Q. The pools containing both PTS^T and Q give rise to the rapid decay while the slower decays are due to pools containing only PTS^T. Analysis of the data gives values for water pool radii which are in agreement with literature values. However, the slow decay of pools containing only PTS^T can be accelerated if migration of Q from other water pools takes place. The kinetics for such processes are described in the Appendix and leads to values for the migration of Cu^{2+} and Fremy's salt among the water pools. Table II gives typical values found, from an analysis given below.

The decay of triplet absorption of 2×10^{-5} M PTS in a micellar solution of 0.2 M AOT in heptane (W_0 = 11, 22, 33) appears exponential, and the calculated first-order rate constant is $< 3 \times 10^3$ s^{-1}. However, when quenchers such as Cu^{2+}, or the nitroxyl radical $(KSO_3)_2NO$ commonly known as Fremy's salt, are added,

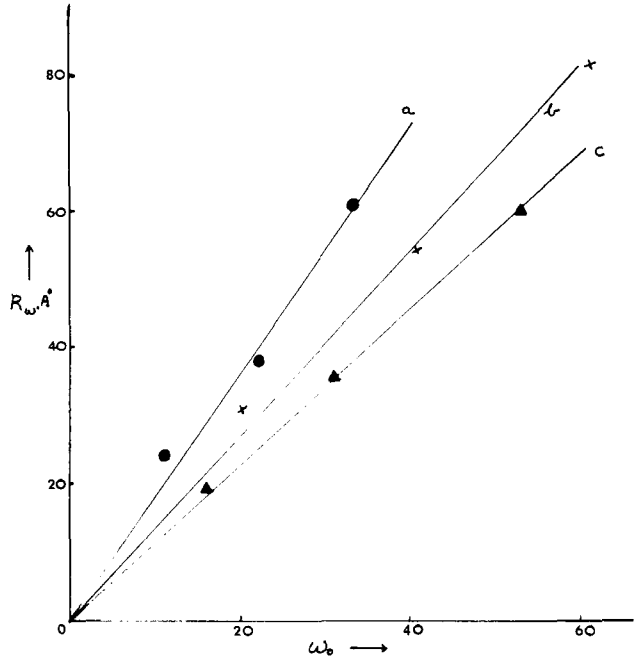

Figure 6. Radii of water pools of several microemulsion systems as determined by analysis of $Ru^{II}(bpy)_3$ luminescence decays in the presence of a quencher, $K_3Fe(CN)_6$ or methyl viologen (MV^{2+}). (a) 0.2 M AOT, heptane, $Fe(CN)_6^{3-}$ as quencher. (b) 1.0 g of CTAB, 2.0 mL of hexanol, 20 mL of dodecane, MV^{2+} as quencher. (c) 1.0 g of potassium oleate, 2.0 mL of hexanol, 5.0 mL of hexadecane, $Fe(CN)_6^{3-}$ as quencher.

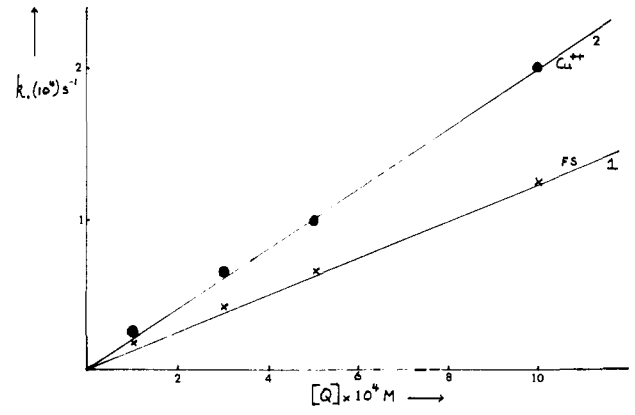

Figure 7. Variation in the inverse of the PTS^T lifetime $1/\tau_t$ with [quencher]. (1) Quencher is Fremy's salt, $k_e = 1.2 \times 10^7$ s^{-1}; (2) quencher is $CuSO_4$, $k_e = 2.0 \times 10^7$ s^{-1}. Solution is 0.2 M AOT/heptane; W_0 = 11; PTS^T observed via absorption at λ = 4250 Å.

Table II. T-T Absorption Decay Analysis for 2.0×10^{-5} M PTS-0.2 M AOT-Heptane

W_0	[FS] $\times 10^3$, M	C_1	$C_2 \times 10^{-4}$, s^{-1}	$C_3 \times 10^{-6}$, s^{-1}	$k_q \times 10^{-5}$, s^{-1}	$k_e \times 10^{-7}$, $L\ M^{-1}\ s^{-1}$
11	1.0	0.65	1.3	1.0	9.0	1.4
	2.0	1.40	2.5	1.0		
22	0.5	0.45	0.40	0.13	0.96	1.0
	1.0	0.90	0.80	0.13		
33	0.5	0.80	0.25	0.012	0.058	1.0

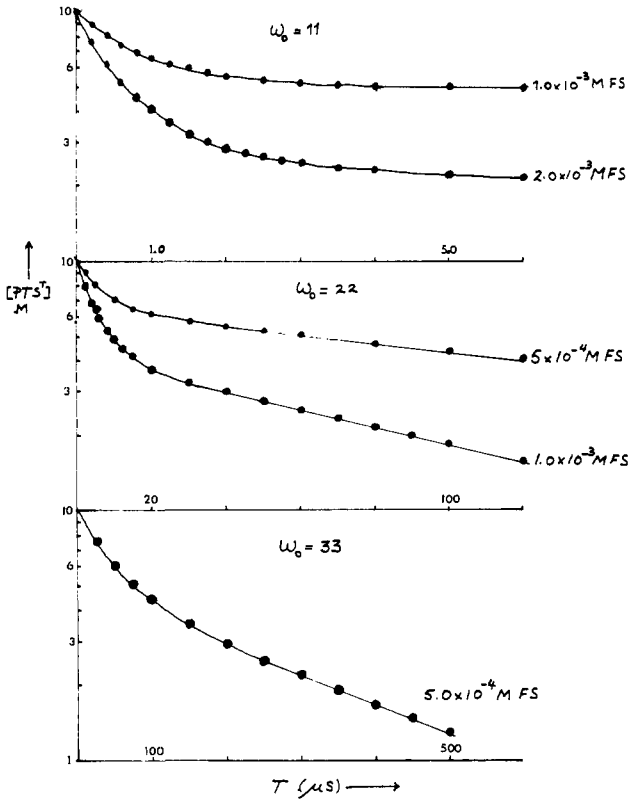

Figure 8. Variation in PTS^T lifetime, $1/\tau_T$, in 0.2 M AOT/heptane, [PTS] = 2.0×10^{-5} with [Fremy's salt] and W_0. PTS^T observed at λ = 4250 Å. Solid lines computer curves from eq 8.

the decay of the excited triplet of PTS becomes nonexponential and consists of two components, a fast component which becomes increasingly slower with increasing water pool size (W_0) and a long component that becomes faster with increasing quencher concentration. The fast decay is attributed to PTS^T present in a water pool containing one or more quenchers, and the slow component due to isolated PTS^T probes in quencher free water pools. The fact that isolated PTS^T decay faster with increasing total quencher concentration is ascribed to transport or exchange of quencher molecules between quencher "filled" and quencher "empty" water pools, exchange that occurs within the lifetime of PTS^T. The time dependence of $[PTS^T]$ for such a kinetic model can be shown to be described by the following expression:[20-23]

$$[PTS^T]_t = [PTS^T]_{t=0} e^{-C_1 t} e^{-C_2(1-e^{-C_3 t})}$$

$$C_1 = k_1 + \frac{k_q}{k_q + k_e[WP]_T} \sum_{n=0}^{\infty} n k_e P_n [WP]_T = k_1 + k_q k_e [Q]_T/(k_q + k_e[WP]_T) \qquad P_n = \bar{n}^n e^{-\bar{n}}/n!$$

$$C_2 = [\bar{n}\, k_q/(k_q + k_e[WP]_T)]^2$$

$$C_3 = k_q + k_e[WP]_T \qquad (10)$$

(21) Atik, S. S.; Singer, L. A. *Chem. Phys. Lett.* **1978**, *59*, 519.
(22) Infelta, P. O.; Grätzel, M.; Thomas, J. K. *J. Phys. Chem.* **1974**, *78*, 190.
(23) Tachiya, M. *Chem. Phys. Lett.* **1975**, *33*, 289.

Table III. Effect of Additives on the Exit Rate Constant, k_e, of Fremy's Salt[a]

additive	$k_e \times 10^{-6}$, $M^{-1}\ s^{-1}$
none	13
0.02 M sodium lauryl sulfate	22
0.02 M sodium laurate	15
0.02 M sodium *p*-tolyl sulfate	18
0.02 M CTAC	3.3
0.02 M tetramethylammonium chloride	6.8
0.3 M hexanol	7.5
0.3 M benzyl alcohol	330
40% benzene	2.5
40% toluene	1.6
none, but dodecane in place of heptane	50

[a] Solution 2.0×10^{-5} M PTS, 0.2 M AOT-heptane, W_0 = 11, 1.0×10^{-3} M Fremy's salt.

where k_1 is the first-order rate constant governing the decay of PTS^T in the absence of quencher, k_q is the intrawater pool first-order quenching rate constant for a water pool that contains only one quencher, and k_e is the bimolecular rate constant for the exchange process that involves water pool collisions.

It is important to note that under conditions where $k_q \gg k_e[WP]_T$, eq 8 reduces to

$$[PTS^T]_t = [PTS^T]_{t=0} e^{-(k_1 + k_e[Q]_T)t} e^{-\bar{n}(1-e^{-k_q t})} \qquad (11)$$

This case is in fact observed for W_0 = 11, where the water pools are small in size. According to eq 11, the limiting linear slope of $\ln([PTS^T]_t/[PTS^T]_{t=0})$ vs. t curve (Figure 8) is given by $k_1 + k_e[Q]_T$ from which k_e could be determined.

Figure 8 shows a good agreement between the experimental data points and the computed curves based on eq 10. The optimal fit was obtained by varying the parameters C_1, C_2, and C_3. Values of k_e for the various reversed micellar AOT systems, W_0 = 11, 22, 33, are given in Table II. These were calculated from the predetermined values of $\bar{n}$ and $[WP]_T$ obtained from the analysis of the luminescence decay of $Ru^{II}(bpy)_3$ in the presence of $Fe(CN)_6^{3-}$. In these experiments exchange of $Fe(CN)_6^{3-}$ between water pools was not observed within the lifetime of the excited charge-transfer state of $Ru^{II}(bpy)_3$, i.e., $k_e[Q]_T \ll 1.54 \times 10^6\ s^{-1}$ so that eq 11 transforms to eq 8.

Effect of Additives on Ion Transport. Table III illustrates the effects of additives on the life time, τ, of PTS^T in a system, 2×10^{-5} M PTS, 0.2 M AOT in heptane with W_0 = 11, [Fremy's salt] = 1.0×10^{-3} M. The increased τ is due to decreased transport of Fremy's salt among the water pools and vice versa.

The data show that the migration of both cationic Cu^{2+} and anionic Fremy's salt behave similarly in all systems. The absolute rate constants for ion transfer are (1/10)–(1/100) smaller than the rate constants for collision of water pools. The latter rate constants are calculated using the Stokes–Einstein relationship where σ is the interaction parameter, D the sum of the diffusion coefficient of the reactants, D_1 the diffusion coefficients of species 1, γ radius of 1, η the viscosity of the medium, R the gas constant, and N_0 is Avogadro's number.

$$k = 4\pi\sigma D, \qquad D_1 = (RT/6\pi\gamma\eta N_0)\ cm^2/s$$

It is suggested that the transport of ions occurs during collisions of the water pools, when the contents of the pools are mixed. The effect of the various additives shown reflects the effect that these additives have on the efficiency of mixing contents of the pools. The most effective additive, however, is benzyl alcohol, which

increases the rate of exchange by 30-fold. It is generally assumed that this molecule tends to locate at the water–hydrocarbon interface, thus causing a disruption of the surfactant head groups at the interface, which, in turn, promotes a more rapid exchange of pool components on pool encounters.

Similar, but smaller, effects are observed with hexanol, SDS, and lauric acid, molecules which should reside at the micelle interface causing disruption of the surface. CTAC and Na_2SO_4 both decrease the rate of solute transfer from one micelle to another. This is probably due to increased cation binding to the anionic surfactant head groups, which, in turn, leads to a more rigid surface. Benzene leads to a greatly decreased rate of solute exchange as significant concentrations of benzene are located in the vicinity of water–hydrocarbon interface. This situation tends to block the movement of solutes through the interface.

Further information on the above effects of added solutes on solute exchange is forthcoming from further studies of the effects of these additives on intramicellar and bulk solvent–micelle reactions.

Intramicelle Reactions. It was shown earlier that $Ru^{II}(bpy)$ in AOT reversed micelles are quenched by $Fe(CN)_6^{3-}$, via fast and slow processes, the fast component arising from the intramicellar reaction. Addition of benzyl alcohol to this system reduces the quenching efficiency some 4-fold, and only one slow decay is observed. It is suggested that the addition of benzyl alcohol causes both $Ru^{II}(bpy)_3$ and $Fe(CN)_6^{3-}$ to enter further into the surfactant layer and away from the aqueous phase. The different environment of the reactants leads to a reduction in the efficiency of the e^- transfer reaction, which gives rise to the quenching.

Micelle–Bulk Reaction. Benzyl alcohol increases the rate of quenching of excited pyrene, which are located in the hydrocarbon bulk, with Tl^+ ions, which are located in the water pools. Again, it is suggested that benzyl alcohol enhances the approach of Tl^+ to the hydrocarbon phase. This facilitates the approach of Tl^+ and excited pyrene which increases the extent of the quenching. The quenching rate constant, in the absence of benzyl alcohol, with $W_0 = 11$–55 and 0.2 M AOT is 3.0×10^8 L M^{-1} s^{-1}, but addition of 0.3 M benzyl alcohol increases k_Q to 4.0×10^9 L M^{-1} s^{-1}, a value close to the diffusion-controlled rate observed in homogeneous solution. In these systems, Tl^+ is aggregated in the water pools, while pyrene is homogeneously distributed in the bulk phase.

Quenching of excited pyrene by the aggregated Tl^+ ions could be envisaged to follow the relationship

$$\frac{1}{\tau_F} = \frac{1}{\tau_F^0} + \sum_{n=1}^{\infty} n k_Q P_n [WP]_T$$

where P_n is the probability of finding a water pool with n quenchers of Tl^+, $[WP]_T$ is the total water pool concentration present in the system, and k_Q is a bimolecular quenching rate constant of excited pyrene by a water pool that contains one quencher.

Regardless of the appropriate statistical distribution function (Poisson or geometric) applicable to the system, the above stated relationship could be easily shown to give

$$1/\tau_F = 1/\tau_F^0 + k_Q[Tl^+]_T$$

The linearity of the plot $1/\tau_F$ vs. total $[Tl^+]$ is in fact born out by experiment for $W_0 = 11$ which gave a value of $k_Q = 2.8 \times 10^8$ m^{-1} s^{-1}. Moreover, in accordance with the kinetic expression given above, but in sharp contrast to the $Ru^{II}(bpy)_3$–$Fe(CN)_6^{3-}$ system (Figure 1), k_Q was found to be independent of the size and $[WP]_T$ as well as [AOT]. Keeping $W_0 = 11$ and varying [AOT] from 0.1 to 0.4 M caused no detectable change in the derived value of k_Q.

Appendix

The following give derivations for the expressions for geometric and Poisson distribution, together with a discussion of the kinetic processes in a geometric distribution of solute among micelles.

The Poisson and geometric distribution functions are derived from a multiequilibrium scheme[17,19] as follows.

Geometric Distribution.

$$D + nQ \underset{k_{-1}}{\overset{k_1}{\rightleftharpoons}} DQ_n \qquad n = 1, 2, 3, \ldots$$

According to this equilibrium scheme, the probability of finding a water pool containing n quenchers is given by

$$G_n = \frac{[DQ_n]}{\sum_{n=0}^{\infty}[DQ_n]}$$

where

$$[DQ_n] = [D](K[Q])^n$$

and

$$K = k_1/k_{-1}$$

$$\sum_{n=0}^{\infty}[DQ_n] = \frac{[D]}{1 - K[Q]}$$

Therefore

$$G_n = (K[Q])^n(1 - K[Q])$$

The following gives a relationship between the mean occupancy number of a water pool ($\bar{n}$) and the term $K[Q]$:

$$\bar{n} = \frac{\sum_{n=1}^{\infty} n[DQ_n]}{\sum_{n=0}^{\infty}[DQ_n]}$$

where

$$\sum_{n=1}^{\infty} n[DQ_n] = [D](K[Q])\left(\sum_{n=1}^{\infty} n(K[Q])^{n-1}\right)$$

Recognizing that $\sum_{n=1}^{\infty} n(K[Q])^{n-1} = 1/(1 - K[Q])^2$ gives $\bar{n}$ as a function of $K[Q]$

$$\bar{n} = K[Q]/(1 - K[Q])$$

Substituting into the expression for G_n yields the geometric distribution function in terms of n and $\bar{n}$

$$G_n = \frac{\bar{n}^n}{(1 + \bar{n})^{n+1}}$$

Poisson Distribution.

$$D + nQ \underset{nk_{-1}}{\overset{k_1}{\rightleftharpoons}} DQ_n \qquad n = 1, 2, 3, \ldots$$

$$[DQ_n] = [D][K[Q]]^n/n!$$

$$\sum_{n=0}^{\infty}[DQ_n] = [D]e^{K[Q]}$$

Therefore the probability of occurrence of a water pool containing n quenchers is given by

$$P_n = (K[Q])^n e^{-K[Q]}/n!$$

Since

$$\bar{n} = \frac{\sum_{n=1}^{\infty} n[DQ_n]}{\sum_{n=0}^{\infty}[DQ_n]} = K[Q]$$

$$P_n = \bar{n}^n e^{-\bar{n}}/n!$$

Kinetics in a Geometric Distribution. The kinetic treatment and formalism that describe intramicellar fluorescence quenching processes and which uses a Poisson function to describe the inhomogeneous distribution of quenchers among the micelles have been previously developed.[20,21] Adopting a similar kinetic model we derive below the appropriate kinetic Stern–Volmer expression

for a geometrical statistical distribution of quenchers among the water pools.

The following are the two additional assumptions used in this model. (1) Both of the reacting species, the fluorescent probes and the quenchers are solubilized exclusively in the water pools. (2) There is an absence of exchange of the reactants between water pools within the time of the excited state reaction. The total concentration of excited probes at time t is given by

$$([P^*]_T)_t = \sum_{n=0}^{\infty}([P^*]_n)_{t=0}e^{-(k_1+nk_q)t} \quad (A1)$$

where $[P_n^*]$ is the concentration of an excited probe located in a water pool containing $\bar{n}$ quencher molecules, k_1 is the sum of all first-order processes leading to the deactivation of P* in the absence of quencher, and k_q is the first-order quenching rate constant that competes with k_1 in the deactivation of P* in a water pool that contains only one quencher.

For a geometric distribution (G_n) of quenchers among the water pools eq A1 becomes

$$([P^*]_T)_t = \sum_{n=0}^{\infty}G_n([P^*]_T)_{t=0}e^{-(k_1+nk_q)t} \quad (A2)$$

where $G_n = \bar{n}^n/(1 + \bar{n})^{n+1}$ and $\bar{n}$ is the average occupancy of a water pool, i.e., $\bar{n} = [Q]_T/[WP]_T$. Upon expansion and rearrangement of eq A2 one obtains

$$([P^*]_T)_t = ([P^*]_T)_{t=0}\left(\frac{e^{-k_1t}}{1+\bar{n}}\right) \times \left[1 + \left(\frac{\bar{n}}{1+\bar{n}}\right)e^{-k_qt} + \left(\frac{\bar{n}}{1+\bar{n}}\right)^2e^{-2k_qt} + \ldots\right] \quad (A3)$$

Recognizing that the infinite series in eq A3 is equivalent to $1/(1 - X)$ where

$$X = [\bar{n}/(1 + \bar{n})]e^{-k_qt}$$

leads to

$$([P^*]_T)_t = ([P^*]_T)_{t=0}e^{-k_1t}/(1 + \bar{n})(1 - X) \quad (A4)$$

which can be further simplified to give

$$([P^*]_T)_t = ([P^*]_T)_{t=0}e^{-k_1t}/[1 + \bar{n}(1 - e^{-k_qt})] \quad (A5)$$

which can be rewritten in the natural log form

$$\ln\left(\frac{([P^*]_T)_t}{([P^*]_T)_{t=0}}\right) = -k_1t - \ln[1 + \bar{n}(1 - e^{-k_qt})] \quad (A6)$$

Note that in cases where $k_q \gg k_1$ and at sufficiently long times such that $k_qt \gtrsim 3$, eq A6 reduces to

$$\ln\left(\frac{([P^*]_T)_t}{([P^*]_T)_{t=0}}\right) = \ln\left(\frac{1}{1+\bar{n}}\right) - k_1t \quad (A7)$$

Equation A7 predicts that in the limit of large t a plot of ln $[([P^*]_T)_t/([P^*]_T)_{t=0}]$ vs. t should be linear with a slope which is equal to the reciprocal of the excited P* life time in the absence of Q, which, when extrapolated to $t = 0$, should give a Y intercept given by $1/(1 + \bar{n})$. On the other hand, according to the Poisson statistical distribution model this intercept would be given simply by $\bar{n}$.

From the estimated value of $\bar{n}$ the total water pool concentration can be calculated which can further be used to determine the "spherical" size of the water pool. It is therefore very important to note that, depending on which statistical distribution is adopted, one could calculate very different values on $\bar{n}$ and therefore $[WP]_T$. Thus, establishing the type of distribution applicable to the system under investigation is essential if this simple and convenient method is to be used to determine a meaningful concentration of such multimolecular aggregates.

Photoinduced Electron Transfer in Organized Assemblies

S. S. Atik and J. K. Thomas*[1]

Contribution from the Department of Chemistry, University of Notre Dame, Notre Dame, Indiana 46556. *Received November 20, 1980*

Abstract: Photoexcitation of the charge-transfer systems pyrene–dimethylaniline and pyrene–dibutylaniline has been studied in several organized assemblies, micelles, microemulsions, and vesicles. Both steady state measurements and pulse laser photolysis date show that the quenching of excited pyrene on the surface by the anilines is rapid but can be described by diffusional-type processes. Detailed mechanisms of the processes are discussed. The main products of the quenching are pyrene anions and dialkylaniline cations. Increasing the size of the assemblies, i.e., micelle to microemulsion, or increasing the rigidity of the reactants' environment, i.e., micelle to vesicle, led to decreased yields of ions. The yields of ions in these latter systems can be restored if polar derivatives of pyrene are used in place of pyrene, thus locating the pyrene chromophore in the region of the assembly surface. Several reactions of the photoproduced pyrene anion were studied, as the lifetime of the anion is sufficiently long (>1 ms) to promote electron transfer between cationic ions such as Eu^{3+} and methyl viologen, in spite of the fact that these ions are strongly repelled by the cationic surfaces of the assemblies. It is concluded that efficient electron transfer and subsequent ion separation only occur when the reactants are located on strongly charged surfaces, where the reactants may move relatively freely, while still remaining bound to the surface. A photodiode effect is suggested to explain the efficient ion separation observed.

Photoinduced electron-transfer processes are of considerable interest in biology and chemistry, and several different systems have been studied from simple aqueous solutions of ions to complex molecules such as chlorophyll. The urgency of alternative sources of energy has given some impetus to studies in this field, as the photoproduction of ions has intriguing possibilities for energy storage. An essential feature for efficient storage of energy is that the photogenerated ions should be prevented from subsequent rapid recombination, a prevalent event in homogeneous media. To this end, simple micellar systems have been used successfully to separate the ions for long periods of time.[2,3] These early data showed

(1) The authors would like to thank the NSF for support of this work under Grant No. CHE 78-24867.

0002-7863/81/1503-3550$01.25/0